

AL- Rafidain
University College

PISSN: (1681-6870); EISSN: (2790-2293)

**Journal of AL-Rafidain
University College for Sciences**

Available online at: <https://www.jruc.s.iq>

JRUCS

Journal of AL-Rafidain
University College
for Sciences

Using Statistical Non-Linear Filters for Gaussian Carina Nebula Image Denoising

Assma G. Jaber	Mohammed A. Mohammed
Drasmaa.ghalib@coadec.uobaghdad.edu.iq	Mohamed.a.mohamed@coadec.uobaghdad.edu.iq
Department of Statistics, College of Administration and Economics, University of Baghdad, Baghdad, Iraq	

Article Information

Article History:

Received: February, 16,
2024

Accepted: April, 12, 2024

Available Online: 31,
December, 2024

Keywords:

Image Denoising; Image
Restoration; Gaussian
Noise; Non-Local Means
Filter; Bilateral Filter.

Abstract

Noise affects images by distorting the features or reducing the required information. Gaussian noise is one of many types of noise that are characterized by normal distribution's statistical properties. Removing or reducing this noise is an essential step in image processing. James Webb Space Telescope (JWST) is a crucial tool for advancing our understanding of the universe across various domains. The images taken by the (JWST) are not only scientifically valuable for advancing our understanding but also have the potential to captivate and inspire people around the world. In this paper, we introduce several nonlinear filters, including Non-Local Mean (NLM) which gives weights to the pixels based on the distance from the noisy pixel. A Bilateral filter that gives weights for each pixel and then calculates the weighted distance. Propose a nonlinear filter depends on obtaining an appropriate smoothing parameter for the image by using the plug-in method and using it to estimate the image's density function, then using an appropriate noise reduction method on the estimated density function to extract the denoised image by removing the Gaussian noise from the Carina Nebula Image, the first image taken by (JWST) on 12 July 2022. The importance of this image lies in its potential to advance scientific knowledge, showcase technological prowess, inspire the public, and contribute to the broader mission of exploring and understanding the cosmos, Also, since it is the farthest point in the universe that humanity has been able to reach or take pictures of, it is therefore essential to preserve its quality to study all its elements or details. These nonlinear filters were therefore selected to highlight the significance of selecting the right technique that can handle, process, and preserve as many details as possible. They also elucidate the degree of advancement achieved in denoising and the distinction between the classical filters and the more sophisticated ones that have evolved to handle finer details. These filters consider the similarities and distances between the central pixel and its neighbours, they preserve the edges of the image as advanced features. Based on quality measurements Peak Signal to Noise Ratio (PSNR) and Structural similarity index measure (SSIM), the filter results were compared and show that the proposed filter gives high performance in restoring images under different Gaussian noise densities. Where it gives values of (42.51) and (0.99) for (PSNR) and (SSIM) respectively, then the bilateral filter gives (30.65) and (0.93) respectively.

Correspondence:

Mohammed A.

Mohammed

Mohamed.a.mohamed@coadec.uobaghdad.edu.iq
DOI: <https://doi.org/10.55562/jruc.s.v56i1.39>

Introduction

In many life applications, satellite images are crucial because they provide a precise and unambiguous image of the subject being studied (Abdul Wadood & Ghalib, 2018; Abdul Wadood & Ghalib, 2019). Examples of these applications include tracking the motion of galaxies, planets, and celestial objects and the degree of climate change and rising and falling ocean water levels. The satellite image is a digital image that is displayed as a series of numbers that can be saved and managed by a digital computer (Muslim & Ghalib, 2019; Ghalib & Abdul Wadood 2020). To translate an image into numbers, it is divided into tiny pieces known as pixels (Muslim & Ghalib, 2019). As with other image types, noise from transmission and acquisition affects satellite images (Kolhe & Yogendra, 2013). This could affect studies and image analysis. Reducing or eliminating the noise is essential for assessing and scrutinizing the image(s). According to (Swamy & Kulkarn; 2020), noise in satellite images is an undesirable physical phenomenon that arises from variations in atmospheric layers. Mention that noise comes in different forms, the most common of which is Gaussian noise (Hambal & Faustini, 2017). According to (Liu & Jianbin; 2018), each pixel in the noisy image is the sum of the true pixel value and a random noise value distributed according to the Gaussian distribution. Additive White Gaussian Noise (AWGN) is the term used to describe this statistical noise, which has a normal distribution-like probability density function (Ali, 2018).

The emergence of noise on telescope images during the acquisition or transmission process is the topic of discussion in this paper. This phenomenon reduces the quality of the images and, as a result, the quality of the analysis and interpretation. With space telescope images being so important for scientific research and studies, the objective is to reduce this noise by using nonlinear techniques to preserve as much information as possible about space telescope pictures. The nonlocal Mean (NLM) and Bilateral (BF) filters are the best for image denoising and edge preservation. (NLM) denoising techniques, finding nearby pixels within a large search window, and calculating the weight of each pixel by comparing and averaging its intensities and similarities (Anh, 2014). These algorithms were developed by Buades et al (Wilson & Julia, 2013). In contrast, Manduchi's (Tomasi & Manduchi, 2005) straightforward, steady, and noniterative bilateral filter (BF) accounts for changes in both spatial and intensity from the central pixel while minimizing noise and avoiding edges (Angulo, 2013). Furthermore, we put forth a successful image-handling method that considers the impact of additional noise on individual image pixels. Each image element's proper smoothing parameter must be chosen, the image's Gaussian density function must be estimated using that parameter, and the estimated Gaussian function must then be subjected to a noise reduction technique. Many researchers have attempted to use these filters in their studies to lower noise in recent years. These studies illuminate the most notable results in the field of digital image denoising, using the filters used in this paper. As a result, by leveraging the features and enhancements made to them, we can apply these techniques to our intended research objective and enhance their performance. For instance, (Arabi & Habib; 2020) discovered that the SNR quality measurement increased from 25.1 when employing Gaussian filtering to 28.8 when utilizing the MRNLM technique, which employed multiple reconstruction NLM filtering (MRNLM) to eliminate redundant information from auxiliary images. (Heo et al.; 2020) carried out a systematic review to evaluate the NLM denoising algorithm's efficacy in MR imaging, demonstrating an accurate method for disease diagnosis. Their findings imply that the NLM denoising algorithm is a practical strategy. More perceptive results are expected from enhanced methods based on fast or optimization terms and various functions. Based on the relativity of the Gaussian adaptive bilateral filter, (Feng & Zhongliang; 2021) proposed a new three-step algorithm for improving infrared images. The recommended algorithm successfully increases the contrast of infrared images by multiplying the image by the suggested weight coefficient, dividing it by the relativity of the Gaussian-adaptive bilateral filter, and combining the processed base layer and detail layer. (Chen & Jing; 2022) proposed an NLM algorithm based on the fractional compact finite difference scheme (FCFDS) to reduce speckle noise in OCT images. When compared to integer order difference operators, FCFDS uses more local pixel data. Simulations demonstrate that, in comparison to other

cutting-edge despeckling techniques, the suggested method significantly reduces noise and preserves image details. (Wagner et al.; 2022) proposed a hybrid denoising technique that combines a convolutional deep learning denoising network with a set of trainable joint bilateral filters (JBFs) to predict the guidance image. The outcome demonstrates a high level of noise reduction efficacy. Appropriate parameter selection is essential for the whale optimization algorithm (WOA), a bilateral filter for image denoising that (Nabahat et al.; 2022) propose. The bilateral filter cannot function effectively unless the parameters are chosen with care. The WOA algorithm optimizes the filter's parameters by designing the filter using the weighted sum of PSNR and SSIM as a fitness function. The results show that the recommended approach performs better than the others. (Wagner et al.; 2022) proposed a bilateral filter that can be integrated into any deep learning algorithm and optimized purely through data-driven means by computing the gradient flow toward its input and hyperparameters. The suggested approach can rival cutting-edge denoising architectures. (Huihua et al.; 2023) Extracted gradient information from images more accurately by combining the Laplacian of the Gaussian operator with an enhanced NLM denoising algorithm. To recover CT images with a high PSNR, the suggested algorithm suppresses noise while maintaining the image edge.

Non-Local Mean Filter (NLM):

The Non-Local Mean Filter (NLM) algorithm was first introduced by A. Buades and is based on a non-local averaging of all pixels (Sarker; 2012); (Dore & Cheriet; 2009). This nonlinear filter, according to (Angella & Rini; 2019), is used to remove Gaussian noise from images while preserving image details. For a pixel (i) in the noise image $v = v\{v(i) \mid i \in I\}$, the estimated value $NL[v](i)$ is calculated as.

$$NL[v] = \sum_{j \in I} w(i, j)v(j) \tag{1}$$

The weights, denoted by $w(i, j)$, are determined by the similarity between pixels (i) and (j) and must meet the standard conditions $0 \leq w(i, j) \leq 1$ and $\sum_j w(i, j) = 1$ (Buades et al; 2005). When the intensity of the vectors $v(N_i)$ and $v(N_j)$ is similar, the two pixels (i) and (j) are similar. (NK) denotes a fixed-size square neighborhood centered at a pixel (k). The similarity is quantified as a decreasing function of the weighted Euclidean distance.

$$\|v(N_i) - v(N_j)\|_{2,a}^2 \tag{2}$$

In noisy neighborhoods, the Euclidean distance increases the following equality (Kommineni; 2019).

$$\|v(N_i) - v(N_j)\|_{2,a}^2 = \|v(N_i) - v(N_j)\|_{2,a}^2 + 2\sigma^2 \tag{3}$$

Since the order of similarity between pixels is expected to be conserved by the Euclidean distance, it clarifies the robustness of the (NLM) (You & Nam; 2013). The definition of the weights is:

$$w(i, j) = \frac{1}{Z(i)} e^{-\frac{\|v(N_i) - v(N_j)\|_{2,a}^2}{h^2}} \tag{4}$$

Where $Z(i)$ is the normalizing constant and (h) is the filtering degree or smoothing parameter.

$$Z(i) = \sum e^{-\frac{\|v(N_i) - v(N_j)\|_{2,a}^2}{h^2}} \tag{5}$$

It regulates the weights' decay as a function of Euclidean distances by controlling the exponential function's decay. This image filter's implementation method is explained by the algorithm that follows.

Step 1:Input the colour image “Carina Nebula”.

Step 2:Add Gaussian noise to the input image with a mean and sigma to obtain a noisy image.

Step 2: Convert the noisy image from RGB colour space to YUV colour space to obtain a YUV image.

Step 3: Extract the luminance channel Y from the YUV image.

Step 4: Apply NLM filtering to the luminance channel Y by calculating the similarity to obtain a filtered luminance channel FY.

Step 5: Replace the original luminance channel Y with the filtered luminance channel FY.

Step 6: Convert the filtered YUV back to RGB colour space to obtain the denoised colour image.

Step 7: Output the denoised colour image.

Bilateral Filter (BF):

Bilateral is a nonlinear filter used to preserve edges and smooth out images. As stated by (Liu et al.;2020), (Anchal et al.; 2018). It uses a different kernel to measure proximity in intensity space, in contrast to traditional convolutional filters (Ghosh et al., 2018). (BF) stands for a weighted average of adjacent pixels (Chen et al., 2020).

$$BF[I]_p = \frac{1}{W_p} \sum_{q \in S} G_{\sigma_s}(\|p - q\|) G_{\sigma_r}(\|I_p - I_q\|) I_q \quad (6)$$

Where (W_p) is the normalization factor, which is defined as follows (Kaur & Bhawna, 2020):

$$W_p = \sum_{q \in S} G_{\sigma_s}(\|p - q\|) G_{\sigma_r}(\|I_p - I_q\|) I_q \quad (7)$$

The parameters σ_s and σ_r dictate the level of filtering that is applied to the image (I). When (q) pixels' intensity values differ from (I_p), the Gaussian range G_{σ_s} reduces their impact. G_{σ_s} is a Gaussian weight that is employed to lessen the effect of distant pixels. The following algorithm explains how this image filter is implemented.

Step 1: Input the colour image "Carina Nebula".

Step 2: Add Gaussian noise to the input image with a mean and sigma to obtain a noisy image.

Step 2: Convert the noisy image from RGB colour space to YUV colour space to obtain a YUV image.

Step 3: Extract the luminance channel Y from the YUV image.

Step 4: Apply bilateral filtering to the luminance channel Y by measuring proximity in intensity to obtain a filtered luminance channel FY.

Step 5: Replace the original luminance channel Y with the filtered luminance channel FY.

Step 6: Convert the filtered YUV back to RGB colour space to obtain the denoised colour image.

Step 7: Output the denoised colour image.

Proposed Filter

Our **Proposed** filter works on converting the image from (**R, G, B**) to (**Y, U, V**) colour space, where the (**Y, U, V**) is a colour representation commonly used in digital image and video processing (Podpora, 2014). It separates the luminance (brightness) information (**Y** component) from the chrominance (colour) information (**U** and **V** components) in an image. By separating the luminance and chrominance components, the **YUV** colour space allows for efficient compression of colour information in image and video data, as human perception is more sensitive to changes in brightness than colour changes (Podpora et al., 2014). A bandwidth selection method applies to the **Y** channel. In nonparametric estimation techniques, choosing the bandwidth, also referred to as the smoothing parameter, is an essential step (Azzabou et al, 2007). To control the blurring or smoothing effect of the kernel function, the appropriate bandwidth parameter must be selected (Hussein, 2022). The bandwidth selection has a significant impact on the quality and accuracy of the estimated function. An overly broad bandwidth may lead to an estimate that is too smooth and overlooks important structures or features in the data (Chiu, 1996). On the other hand, an estimate with an excessively narrow bandwidth may exhibit a high degree of noise and may reflect the distinctive characteristics of each data point rather than the underlying pattern (Loader, 1999). There are several ways to choose your bandwidth, including (plug-in) techniques. One method used

in nonparametric density estimation, specifically in kernel density estimation, is the bandwidth selection (plug-in) method (Chu, 2015). By minimizing a selected criterion or objective function, the optimal bandwidth is estimated using the (plug-in) method. According to Chacón (2009), these criteria evaluate how well the estimated density fits the observed data, and the best bandwidth is determined by minimizing the criterion of choice. The (plug-in) method seeks to achieve an appropriate degree of smoothing for the given data by balancing over- and under-smoothing the density estimate by plugging in the estimated optimal bandwidth (Oliveira, 2012). **Plug-in** bandwidth selectors are a major class of bandwidth selectors that are derived from the (AMISE) expansion (Ibraheem, 2012). The $R(f'')$ in (\mathbf{h}_{AMISE}) is replaced by an estimate by choosing a pilot Bandwidth (b) to get $R(\hat{f}_b'')$ An initial density estimate, commonly from the Gaussian kernel, is used to estimate h . This value is plugged into the (\mathbf{h}_{AMISE}) and computed (Florence, 2019). The result will be:

$$h_{\text{plug-in}} = \left[\frac{R(K)}{nR(\hat{f}_b'')m_2^2} \right]^{\frac{1}{5}} \tag{8}$$

After we get the bandwidth for the Y channel, we use it for density estimation, where the kernel density estimation (**KDE**) is a non-parametric method used to estimate the probability density function (**PDF**) of a random variable based on a set of observed data points (Hang, 2016). Gaussian kernel density estimation is a specific type of (**KDE**) that uses a Gaussian distribution as the kernel function (Węglarczyk, 2018). In kernel density estimation, the estimated density at any point x is formulated as (Dubeya, 2022).

$$\hat{f}_h(x) = \frac{1}{n} \sum_{i=1}^n K\left(\frac{x - X(i)}{h}\right) \tag{9}$$

Where $x(i)$ is a neighbouring point to x , n is the number of neighbours, $K(\cdot)$ is the kernel function, and (h) is its bandwidth also called the smoothing constant. The kernel function can be considered a weighting factor that gives a larger value when $x(i)$ is close to x .

Finally, we apply a denoising method to the Gaussian kernel density function. Wavelet Shrinkage also called wavelet threshold algorithm is a nonlinear denoising method (Liu, 2023). The key step in the threshold denoising method based on wavelet transform is to process the decomposed wavelet coefficients by setting a threshold. Then, we get estimated wavelet coefficients (Lin, 2017). These wavelet denoising methods suppress the noisy coefficient magnitudes while keeping the local structures. Ideally, only the wavelet coefficients that correspond to the noise component should be removed, whereas the coefficients containing a significant structure component should be reduced (Singh & Nirvair, 2012). There are two types of thresholds (hard and soft) threshold (Khedkar, 2016). Hard thresholding is the most straightforward technique for implementing wavelet denoising, which interprets the “keep or kill” statement (Kumar, 2014). The wavelet coefficient is set to the vector $\omega_n^{(Ht)}$ with element

$$\omega_n^{(Ht)} = \begin{cases} 0 & \text{if } |\omega_n| \leq \eta \\ \omega_n & \text{if } |\omega_n| > \eta \end{cases} \tag{10}$$

If the coefficients are more significant than the threshold value (η), They remain without changing. However, if they are smaller than or equal to the threshold value (η), They are eliminated or set to zero. On the other hand, soft thresholding which is defined as follows:

$$\omega_n^{(St)} = \text{sign}[\omega_n](\text{ABS}(\omega_n) - \eta) + \dots \tag{11}$$

$$\text{Sign}[\omega_n] = \begin{cases} +1 & \text{if } \omega_n > 0 \\ 0 & \text{if } \omega_n = 0 \\ -1 & \text{if } \omega_n < 0 \end{cases} \tag{12}$$

$$(\text{ABS}(\omega_n) - \eta) = \begin{cases} (\text{ABS}(\omega_n) - \eta) & \text{if } (\text{ABS}(\omega_n) - \eta) \geq 0 \\ 0 & \text{if } (\text{ABS}(\omega_n) - \eta) < 0 \end{cases} \quad (13)$$

Soft thresholding brings all coefficients to zero when the wavelet coefficient is less than the threshold and when the coefficients are more significant than the threshold (η), they persist after reducing by the amount of the threshold. In contrast, the soft threshold is a continuous function is what the statement “Shrink” interprets. This provides the results of the wavelet thresholding estimator. For small samples, hard thresholding has a lower mean square error and less sensitivity to small noises in the data. Soft thresholding has negligible deviation and an overall mean square error (Gilda, 2019).

Discussion of Results

The experiment was carried out by adding AWGN with zero mean and 0.01 variance to the approved image as shown in Figure 1, which is the first James Webb space telescope image taken to the Carina Nebula on July 12, 2022 (<https://webb.nasa.gov/>). With thousands of astronomers using JWST worldwide, JWST is the leading observatory of the coming ten years. It takes images from the first bright lights following the Big Bang to the creation of solar systems that could support life on planets like Earth and the development of our own Solar System, it examines every stage of our Universe's history. So, this image must be clear and free of impurities. Considering the significance of these images, we should work to eliminate any noise that may have been introduced during the transmission and acquisition process. So, in this experiment, we added different percentages of Gaussian noise to the adopted image and then applied the adopted filters, the code of these filters is written using MATLAB.

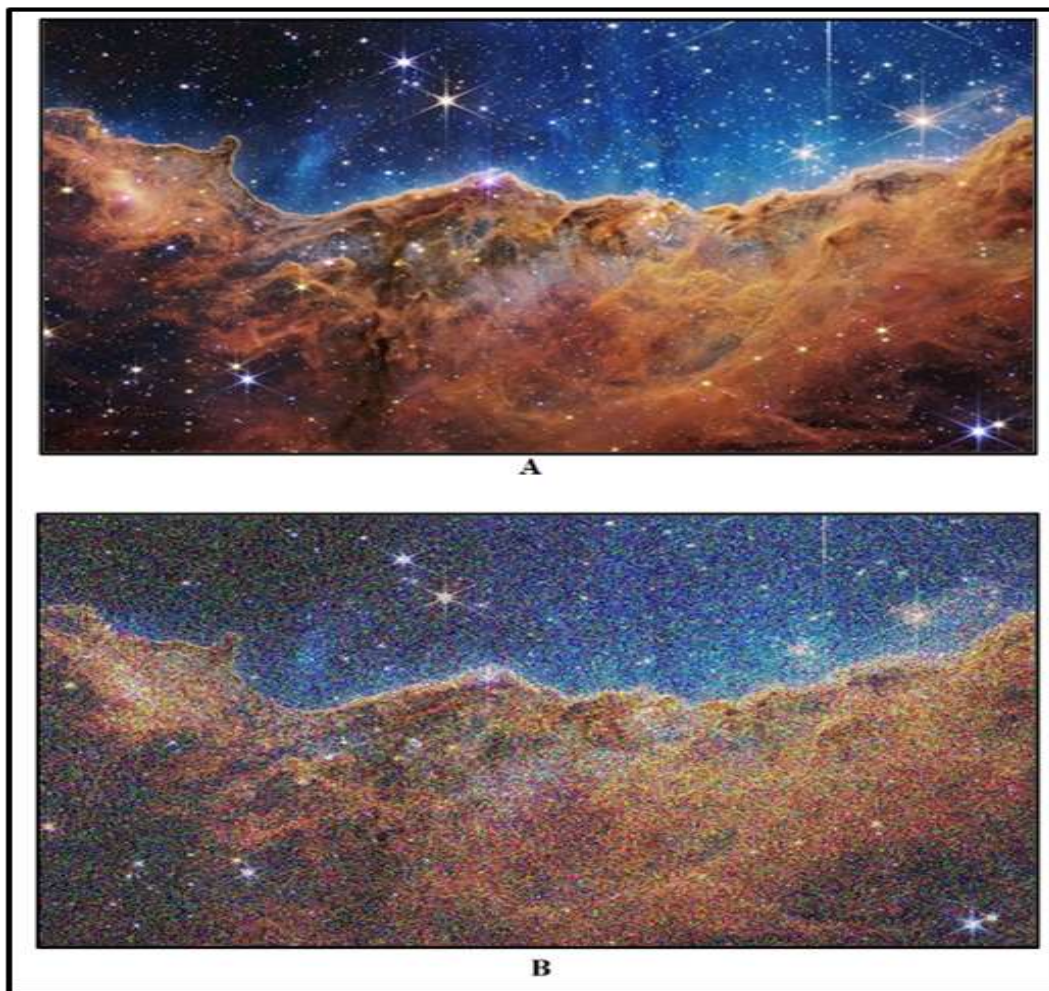


Figure 1: Original Image of Carina Nebula (A), Gaussian Noise Image of Carina Nebula (B).

To evaluate the quality of the obtained results the Structural Similarity Index Measure (SSIM) and the Peak Signal to Noise Ratio (PSNR) are used to calculate this quality. Where (PSNR) is regarded as a quality measurement that is frequently used to quantify reconstruction quality for images and video (Hore & Djemel, 2010):

$$PSNR = 10 * \log_{10} * \left(\frac{255^2}{MSE_{(x,y)}}\right) \tag{14}$$

Where:

$$MSE_{(x,y)} = \frac{1}{MN} \sum_{i=1}^M \sum_{j=1}^n (x_{ij} - y_{ij})^2 \tag{15}$$

On the other hand, (SSIM) is a quality measure that determines how similar the two digital image structures are (Wang et al., 2004). The following equation provides it:

$$SSIM = (l(x, y))^\alpha * (c(x, y))^\beta * (s(x, y))^\gamma \tag{16}$$

Which stand for three weights (Bakurov et al., 2022) with exponents (α), (β), and (γ), respectively.

$$I(x, y) = \frac{2\mu_x\mu_y + C_1}{\mu_x^2 + \mu_y^2 + C_1} \tag{17}$$

$$C(x, y) = \frac{2\sigma_x\sigma_y + C_2}{\sigma_x^2 + \sigma_y^2 + C_2} \tag{18}$$

$$S(x, y) = \frac{\sigma_{xy} + C_3}{\sigma_x\sigma_y + C_3} \tag{19}$$

Where C1, C2, and C3 are small quantities for numerical stability. To assess the efficacy of the approved filters, we added different amounts of Gaussian noise ratios to the image. Where The quality of the restored images varies, as Table 1 illustrates. The results indicate that the proposed filter performs best in terms of both PSNR and SSIM when there is a noise density of 0.01 where it is given the values 42.51 PSNR, and 0.99 SSIM respectively, while the Bilateral filter ranks second with 30.65 PSNR and 0.93 SSIM. According to measurements, Nonlocal mean filters have the values 24.32 PSNR and 0.89 SSIM, respectively. Figure 2 displays the images that have been restored.

Table 1: PSNR and SSIM values for the restored images of each filter

Filters	Image Quality Measurements	
	PSNR	SSIM
Bilateral	30.65	0.93
NLM	24.32	0.89
Proposed	42.51	0.99

When we implement the filters in different noise Ratio (**50%**, **75%**), to denoise the (**Carina Nebula**) image, we get the following results:

Table 2: PSNR and SSIM values of the restored images calculated for different noise ratio

Filters	Image Quality Measurements in Different Noise Ratios			
	50%		75%	
	PSNR	SSIM	PSNR	SSIM
Bilateral	34.63	0.98	34.95	0.98
NLM	13.12	0.80	12.63	0.80
Proposed	37.30	0.99	35.36	0.99

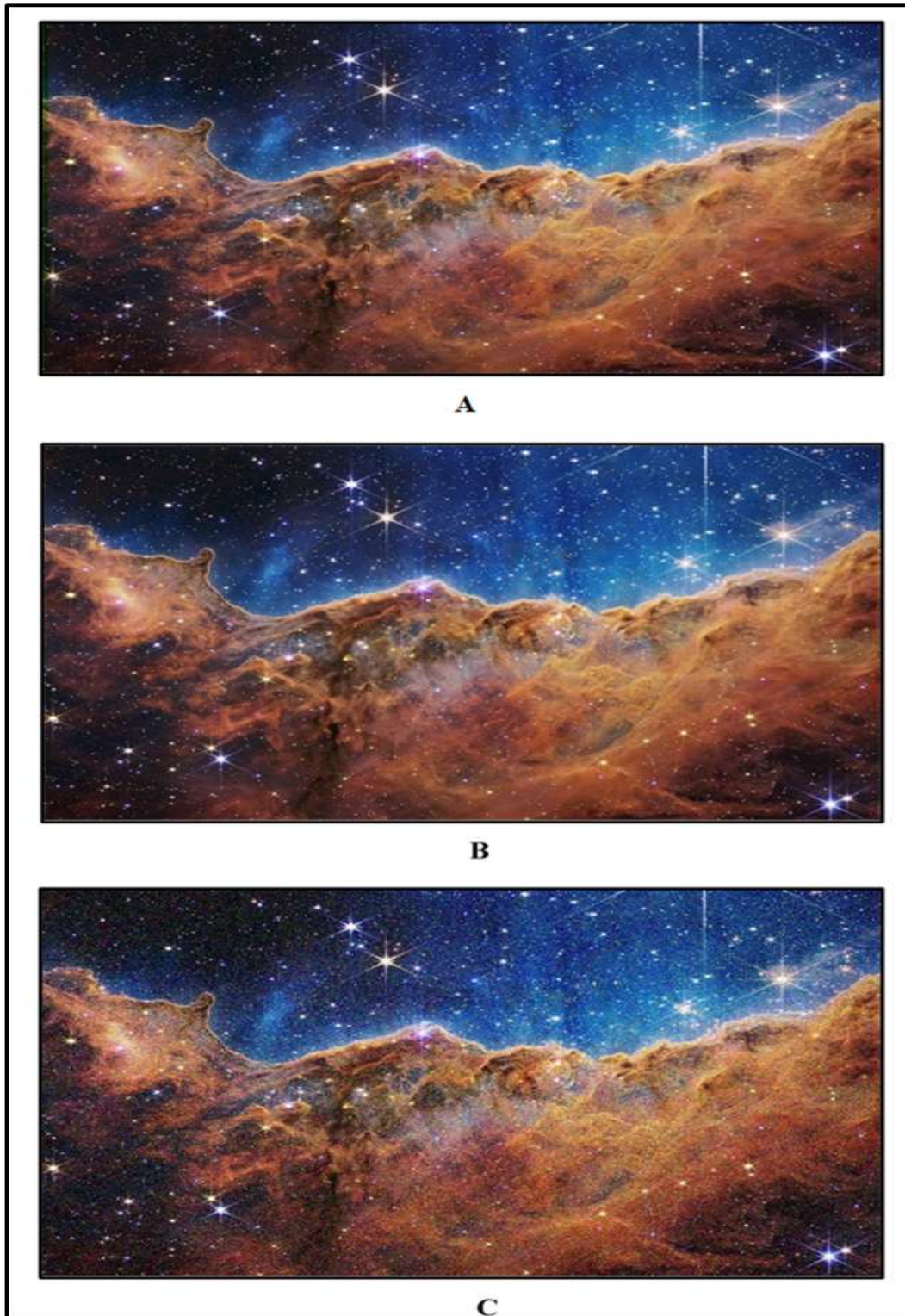


Figure 4: Showing (A) Restored Image of Carina Nebula by Proposed Filter, (B) Restored Image by Bilateral Filter, (C) Restored Image by Nonlocal Mean Filter

We can observe from the results in Table 2 that the order of filters about the restored image quality and the presence of various noise levels did not change. The first filter is the proposed one, which has 37.30 PSNR and 0.99 SSIM in 50% and 35.36 PSNR and 0.99 SSIM in 75% noise density, respectively. The second one is the bilateral filter with 34.63 PSNR, 0.98 SSIM in 50% noise density, 34.98 PSNR, and 0.98 SSIM in 75% noise density.

The mechanism used by the proposed method to analyze the image, which was represented by a series of stages, is what accounts for its superiority. First, an appropriate bandwidth parameter

was extracted using a plug-in method designed to minimize errors. The Gaussian density function was then estimated using this parameter by calculating the mean and variance of the noise contained in the image. Finally, a useful denoising method is to divide the image using thresholding. Because the bilateral filter assigns more weight to pixels that are both spatially close and have similar intensity values, it has the benefit of reducing noise while maintaining image edges. In this manner, critical features are retained while noise is reduced and edges are maintained, giving the filtered image a smoother visual quality. Conversely, the nonlocal mean filter takes into account an image's overall structure and is a flexible and powerful denoising method. However, it requires adjustments and modifications to make it more feasible for use in practical applications because it is computationally demanding.

Conclusion

The outcomes demonstrate how adaptable the suggested filter was in lowering noise levels without sacrificing any of the original image's characteristics. It moved the PSNR almost eleven degrees away from its nearest filter and achieved a high image quality index. Furthermore, the structural similarity quality index (SSIM), which gave the filter a high-efficiency level of 0.93, demonstrates how well the bilateral filter maintains image contrast and edges. This is not to say that the nonlocal mean filter is not effective; in fact, the NLM considers the global structure of the image, providing better preservation of edges and details, but at a higher computational cost, it is regarded as one of the most cutting-edge and effective filters for noise reduction, as demonstrated by its performance. Ultimately, the findings demonstrate that the quality of the restored image decreases with increasing added noise density.

Acknowledgement

The image of the Carina Nebula, the furthest point in the universe that humans can reach, is one of the images from the James Webb space telescope (JWST) that the author is grateful for being provided by the US National Aeronautics and Space Administration Agency (NASA) <https://webb.nasa.gov/>.

References

- [1] Abdul Wadood, M. and Ghalib, A. (2019). Split and Merge Regions of Satellite Images Using the Non-Hierarchical Algorithm of Cluster Analysis. *Journal Of Economics and Administrative Sciences*, Vol. 25, No. 111, pp.466–484. <https://doi.org/https://doi.org/10.33095/jeas.v25i111.1638>.
- [2] Abdul Wadood, M. and Ghalib, A. (2018). Use Some Statistical Algorithms in Mock Hacking Satellite Images. *Journal Of Economics and Administrative Sciences*, Vol. 108, No. 24, pp.474–487.
- [3] Ali, M. (2018). MRI Medical Image Denoising by Fundamental Filters. *High-Resolution Neuroimaging - Basic Physical Principles and Clinical Applications*, Vol. 43, No. 17, pp.658–666. <https://doi.org/10.5772/intechopen.72427>.
- [4] Anchal, A., Sumit, B., Bhawna, G., Ayush, D. and Sunil, A. (2018). An Efficient Image Denoising Scheme for Higher Noise Levels Using Spatial Domain Filters. *Biomedical and Pharmacology Journal*, Vol. 11, No. 2, pp.625–634. <https://doi.org/10.13005/bpj/1415>.
- [5] Angella, S., Ari, S. and Rini, I. (2019). Application of Denoising Non-Local Mean Filter (NLM) in MRI Brain Image T2WI TSE SENSE. *International Journal of Allied Medical Sciences and Clinical Research (IJAMSCR)*, Vol. 7, No. 3, pp.1033–1039.
- [6] Angulo, J. (2013). Morphological Bilateral Filtering. *SIAM Journal on Imaging Sciences*, Vol. 6, No. 3, pp.1790–1822. <https://doi.org/10.1137/110844258>.
- [7] Anh, N. (2014). Image Denoising by Adaptive Non-Local Bilateral Filter. *International Journal of Computer Applications*, Vol. 99, No. 12.

- [8] Arabi, H. and Habib Z. (2020). Non-Local Mean Denoising Using Multiple Pet Reconstructions. *Annals of Nuclear Medicine*, Vol. 35, No. 2, pp.176–186. <https://doi.org/10.1007/s12149-020-01550-y>.
- [9] Azzabou, Noura, Nikos Paragios, Frederic Guichard, and Frederic Cao. “Variable Bandwidth Image Denoising Using Image-Based Noise Models.” *2007 IEEE Conference on Computer Vision and Pattern Recognition*, 2007. <https://doi.org/10.1109/cvpr.2007.383216>.
- [10] Bakurov, I., Marco, B., Raimondo, S., Mauro, C. and Leonardo, V. (2022). Structural Similarity Index (SSIM) Revisited: A Data-Driven Approach. *Expert Systems with Applications*, No. 189. <https://doi.org/10.1016/j.eswa.2021.116087>.
- [11] Buades, A., B. Coll, and Morel, M. (2005). A Non-Local Algorithm for Image Denoising. *IEEE Computer Society Conference on Computer Vision and Pattern Recognition (CVPR '05)*, No. 16. <https://doi.org/10.1109/cvpr.2005.38>.
- [12] Chacón, J. E., and T. Duong. “Multivariate Plug-in Bandwidth Selection with Unconstrained Pilot Bandwidth Matrices.” *TEST* 19, no. 2 (2009): 375–98. <https://doi.org/10.1007/s11749-009-0168-4>.
- [13] Chen, B., Yi-Syuan, T. and Jia-Li, Y. (2020). “Gaussian-Adaptive Bilateral Filter.” *IEEE Signal Processing Letters*, No. 27, pp.1670–1674. <https://doi.org/10.1109/lsp.2020.3024990>.
- [14] Chen, H. and Jing, G. (2022). Non-Local Mean Denoising Algorithm Based on Fractional Compact Finite Difference Scheme Effectively Reduces Speckle Noise in Optical Coherence Tomography Images. *Micromachines*, Vol. 13, No. 12, pp.2039-2039. <https://doi.org/10.3390/mi13122039>.
- [15] Chiu, Shean-Tsong. “A Comparative Review of Bandwidth Selection for Kernel Density Estimation.” *Institute of Statistical Science, Statistica Sinica* 6, no. 1 (January 1996): 129–45.
- [16] Chu, Chi-Yang, Daniel Henderson, and Christopher Parmeter. “Plug-in Bandwidth Selection for Kernel Density Estimation with Discrete Data.” *Econometrics* 3, no. 2 (2015): 199–214. <https://doi.org/10.3390/econometrics3020199>.
- [17] Dore, V. and Cheriet, M. (2009). Robust NL-Means Filter with Optimal Pixel-Wise Smoothing Parameter for Statistical Image Denoising. *IEEE Transactions on Signal Processing*, Vol. 57, No. 5, pp.1703–1716. <https://doi.org/10.1109/tsp.2008.2011832>.
- [18] Dubeya, P. (2022). Comparative Performance Analysis of Spatial Domain Filtering Techniques in Digital Image Processing for Removing Different Types of Noise. *International Journal of Nonlinear Analysis and Applications*, No. 13, pp.117–125.
- [19] Feng, X. and Zhongliang, P. (2021). Detail Enhancement for Infrared Images Based on Relativity of Gaussian-Adaptive Bilateral Filter. *OSA Continuum*, Vol. 4, No. 10, pp.2671-2676. <https://doi.org/10.1364/osac.434858>.
- [20] Florence, Kimari, Adem Aggrey, and Kiti Leonard. “Efficiency of Various Bandwidth Selection Methods across Different Kernels.” *IOSR Journal of Mathematics (IOSR-JM)* 15, no. 3 (June 2019): 55–62.
- [21] Ghalib, A. and Abdul Wadood, M. (2020). Using Multidimensional Scaling Technique in Image Dimension Reduction for Satellite Image. *Periodicals of Engineering and Natural Sciences*, Vol. 8, No. 1, pp.447–454. <http://dx.doi.org/10.21533/pen.v8i1.1171>.
- [22] Ghosh, S., Pravin, N. and Kunal, C. (2018). Optimized Fourier Bilateral Filtering. *IEEE Signal Processing Letters*, Vol. 25, No. 10, pp.1555–1559. <https://doi.org/10.1109/lsp.2018.2866949>.
- [23] Gilda, Sankalp, and Zachary Slepian. “Automatic Kalman-Filter-Based Wavelet Shrinkage Denoising of 1d Stellar Spectra.” *Monthly Notices of the Royal Astronomical Society* 490, no. 4 (2019): 5249–69. <https://doi.org/10.1093/mnras/stz2577>.
- [24] Hambal, A., Zhijun, P. and Faustini, I. (2017). Image Noise Reduction and Filtering Techniques. *International Journal of Science and Research (IJSR)*, Vol. 6, No. 3, pp.2033–2038. <https://doi.org/10.21275/25031706>.

- [25] Hang, Hanyuan, Ingo Steinwart, Yunlong Feng, and Johan A.K. Suykens. "Kernel Density Estimation for Dynamical Systems." *Journal of Machine Learning Research* 1 (July 2016): 1–49. <https://doi.org/10.48550/arXiv.1607.03792>.
- [26] Heo, Y., Kyuseok, K. and Youngjin, L. (2020). Image Denoising Using Non-Local Means (NLM) Approach in Magnetic Resonance (MR) Imaging: A Systematic Review. *Applied Sciences*, Vol. 10, No. 20, pp.7028-7028. <https://doi.org/10.3390/app10207028>.
- [27] Hore, A. and Djemel, Z. (2010). Image Quality Metrics: PSNR vs. SSIM. *2010 20th International Conference on Pattern Recognition*. No. 22. <https://doi.org/10.1109/icpr.2010.579>.
- [28] Huihua, K., Gao, W. and Di, Y. (2023). An Improved Non-Local Means Algorithm for CT Image Denoising, No. 25. <https://doi.org/10.21203/rs.3.rs-2915903/v1>.
- [29] Hussein, Mohammad M. Fage. "Comparison of Time Series Models before and after Using Wavelet Shrinkage Filtering to Forecast the Amount of Natural Gas in Iraq." *Cihan University-Erbil Scientific Journal (CUESJ)* 6, no. 1 (2022): 32–46.
- [30] Ibraheem, Noor A., Mokhtar M. Hasan, Rafiqul Z. Khan, and Pramod K. Mishra. "Understanding Color Models: A Review." *ARNP Journal of Science and Technology* 2, no. 3 (April 2012): 265–75.
- [31] Kaur, B., Ayush, D. and Bhawna G. (2020). Comparative Analysis of Bilateral Filter and Its Variants for Magnetic Resonance Imaging. *The Open Neuroimaging Journal*, Vol. 13, No. 1, pp.21–29. <https://doi.org/10.2174/1874440002013010021>.
- [32] Kolhe, Y. and Yogendra, J. (2013). Removal of Salt and Pepper Noise from Satellite Images. *International Journal of Engineering Research and Technology (IJERT)*, Vol. 2, No. 11, pp.2051–2058. <https://doi.org/10.17577/IJERTV2IS110634>.
- [33] Khedkar, Sameer, Kalyani Akant, and Milind M. Khanapurkar. "IMAGE DENOISING USING WAVELET TRANSFORM." *International Journal of Research in Engineering and Technology* 5, no. 4 (April 2016): 206–12.
- [34] Kommineni, V. and Hemantha, K. (2019). Image Denoising Techniques. *International Journal of Recent Technology and Engineering (IJRTE)*, Vol. 7, No. 5, pp. 417–419.
- [35] Kumar, P. (2014). Image Filtering Using Linear and Non-Linear Filter for Gaussian Noise. *International Journal of Computer Applications*, Vol. 93, No. 8, pp. 29–34, <https://doi:10.5120/16237-5760>.
- [36] Lin, Lin, and Liangang Feng. "Comparative Analysis of Image Denoising Methods Based on Wavelet Transform and Threshold Functions." *International Journal of Engineering* 30, no. 3 (February 2017): 199–206.
- [37] Liu, B. and Jianbin, L. (2018). Non-Local Mean Filtering Algorithm Based on Deep Learning. *MATEC Web of Conferences*, Vol. 23, No. 2. <https://doi.org/10.1051/mateconf/201823203025>.
- [38] Liu, C. and Li, Z. (2023). A Novel Denoising Algorithm Based on Wavelet and Non-Local Moment Mean Filtering. *Electronics*, Vol. 12, No. 6. <https://doi.org/10.3390/electronics12061461>.
- [39] Liu, W., Pingping, Z., Xiaogang, C., Chunhua, S., Xiaolin, H. and Jie, Y. (2020). Embedding Bilateral Filter in Least Squares for Efficient Edge-Preserving Image Smoothing. *IEEE Transactions on Circuits and Systems for Video Technology*, Vol. 30, No. 1, pp.23–35. <https://doi.org/10.1109/tcsvt.2018.2890202>.
- [40] Loader, Clive R. "Bandwidth Selection: Classical or Plug-In?" *The Annals of Statistics* 27, no. 2 (1999). <https://doi.org/10.1214/aos/1018031201>.
- [41] Muslim, A. and Ghalib, A. (2019). Comparison Between the Method of Principal Component Analysis and Principal Component Analysis Kernel for Imaging Dimensionality Reduction. *Journal Of Economics and Administrative Sciences*, Vol. 16, No. 2, pp.11–24. <https://doi.org/https://doi.org/10.33899/ijqjoss.2019.164189>.
- [42] Muslim, A. and Ghalib, A. (2019). Use Principal Component Analysis Technique to Dimensionality Reduction to Multi-Source. *Journal Of Economics and Administrative*

- Sciences*, Vol. 25, No. 115, pp.464–473.
<https://doi.org/https://doi.org/10.33095/jeas.v25i115.1778>.
- [43] Nabahat, M., Farzin, K. and Nima, N. (2022). Optimization of Bilateral Filter Parameters Using a Whale Optimization Algorithm. *Research in Mathematics*, Vol. 9, No. 1. <https://doi.org/10.1080/27684830.2022.2140863>.
- [44] Oliveira, M., R.M. Crujeiras, and A. Rodríguez-Casal. “A Plug-in Rule for Bandwidth Selection in Circular Density Estimation.” *Computational Statistics & Data Analysis* 56, no. 12 (2012): 3898–3908. <https://doi.org/10.1016/j.csda.2012.05.021>
- [45] Podpora, Michal, Grzegorz Paweł Korbaś, and Aleksandra Kawala-Janik. “YUV vs RGB—Choosing a Color Space for Human-Machine Interaction.” *Annals of Computer Science and Information Systems*, 2014. <https://doi.org/10.15439/2014f206>.
- [46] Sarker, S. (2012). Use of Non-Local Means Filter to Denoise Image Corrupted by Salt and Pepper Noise. *Signal and amp Image Processing: An International Journal*, Vol. 3, No. 2, pp.223–235. <https://doi.org/10.5121/sipij.2012.3217>.
- [47] Singh, I. and Nirvair, N. (2014). Performance Comparison of Various Image Denoising Filters under Spatial Domain. *International Journal of Computer Applications*, Vol. 96, No. 19, pp.21–30. <https://doi:10.5120/16903-6969>.
- [48] Swamy, S. and Kulkarn, P. (2020). A BASIC OVERVIEW OF IMAGE DENOISING TECHNIQUES. *International Research Journal of Engineering and Technology (IRJET)*, Vol. 7, No. 5, pp.850–857.
- [49] Tomasi, C. and Manduchi, R. (2005). Bilateral Filtering for Gray and Color Images. *Sixth International Conference on Computer Vision (IEEE Cat. No.98CH36271)*. Vol 22, No. 16. <https://doi.org/10.1109/iccv.1998.710815>.
- [50] Wagner, F., Mareike, T., Felix, D., Mingxuan, G., Mayank, P., Stefan, P., Noah, M., Laura, P., Yixing, H. and Andreas, M. (2022). Trainable Joint Bilateral Filters for Enhanced Prediction Stability in Low-Dose CT. *Scientific Reports*, Vol. 12, No. 1. <https://doi.org/10.1038/s41598-022-22530-4>.
- [51] Wagner, F., Mareike, T., Mingxuan, G., Yixing, H., Sabrina, P., Mayank, P. and Stefan, P. (2022). Ultralow-parameter Denoising: Trainable Bilateral Filter Layers in Computed Tomography. *Medical Physics*, Vol. 49, No. 8, pp.5107–5120. <https://doi.org/10.1002/mp.15718>.
- [52] Wang, Z., Bovik, C. Sheikh, R. and Simoncelli, P. (2004). Image Quality Assessment: From Error Visibility to Structural Similarity. *IEEE Transactions on Image Processing*, vol. 13, No. 4, pp.600–612. <https://doi.org/10.1109/tip.2003.819861>.
- [53] Węglarczyk, Stanisław. “Kernel Density Estimation and Its Application.” *ITM Web of Conferences* 23 (2018): 00037. <https://doi.org/10.1051/itmconf/20182300037>.
- [54] Wilson, B. and Julia, D. (2013). A Survey of Non-Local Means Based Filters for Image Denoising. *International Journal of Engineering Research and Technology (IJERT)*, Vol. 2, No. 10, pp.3768–3771.
- [55] You, J. and Nam, C. (2013). An Adaptive Bandwidth Nonlocal Means Image Denoising in Wavelet Domain. *EURASIP Journal on Image and Video Processing*, No. 1. <https://doi.org/10.1186/1687-5281-2013-60>.



AL-Rafidain
University College

PISSN: (1681-6870); EISSN: (2790-2293)

مجلة كلية الرافدين الجامعة للعلوم

Available online at: <https://www.jruc.s.edu.iq>

JRUCS

Journal of AL-Rafidain
University College
for Sciences

استخدام المرشحات الإحصائية غير الخطية لتقليل الضوضاء الغاوسية من صورة سديم كارينا

محمد عبد الودود محمد	أسماء غالب جابر
Mohamed.a.mohamed@coadec.uobaghdad.edu.iq	Drasmaa.ghalib@coadec.uobaghdad.edu.iq
قسم الاحصاء، كلية الإدارة والاقتصاد، جامعة بغداد، بغداد، العراق	

المستخلص

تؤثر الضوضاء على الصور عن طريق تشويه الميزات أو تقليل المعلومات المطلوب، وتعد الضوضاء الغوسية إحدى أكثر أنواع الضوضاء شيوعاً وهي تتميز بالخصائص الإحصائية للتوزيع الطبيعي، وعملية إزالة هذا الضوضاء أو تقليله خطوة أساسية في معالجة الصور، يعد تلسكوب جيمس ويب الفضائي (JWST) أداة حاسمة لتعزيز فهمنا للكون عبر مختلف المجالات، إذ تعتبر الصور التي يلتقطها التلسكوب ليست ذات قيمة علمية لتعزيز فهمنا فحسب، بل لديها أيضاً القدرة على جذب وإلهام الناس في جميع أنحاء العالم. قدما في هذا البحث عدة مرشحات غير خطية بما في ذلك المتوسط غير المحلي (NLM) الذي يعطي أوزان للعناصر الصورية اعتماداً على المسافة من العنصر الصوري المتأثر بالضوضاء، وإيضاً المرشح الثنائي الذي يعطي أوزاناً لكل عنصر صوري من ثم يحسب المسافة الموزونة الفاصلة بينهم، واقترحنا مرشح غير خطي يعتمد على استخراج معامل تنعيم مناسب للصورة باستخدام طريقة plug-in واستخدامها لتقدير دالة كثافة الصورة، ثم يستخدم أسلوب تنعيم أو تقليل ضوضاء مناسب لتقليل الضوضاء الغاوسية من دالة الكثافة المقدر لاستخراج صورة سديم كارينا مخفضة الضوضاء، وهي الصورة الأولى الملتقطة بواسطة (JWST) في 12 يوليو 2022. وتكمن أهمية هذه الصورة في قدرتها على التقدم في المعرفة العلمية وإظهار البراعة التكنولوجية وإلهام الجمهور والمساهمة في المهمة الأوسع المتمثلة في استكشاف وفهم الكون، كما أنها تعد أبعد نقطة في الكون تمكنت البشرية من الوصول إليها أو التقاط صور لها، لذلك من الضروري للحفاظ على جودتها لدراسة جميع عناصرها أو تفاصيلها، ولذلك تم اختيار المرشحات غير الخطية هذه لتسليط الضوء على أهمية اختيار التقنية المناسبة التي يمكنها التعامل مع أكبر عدد ممكن من التفاصيل ومعالجتها والحفاظ عليها، كما أنها توضح درجة التقدم الذي تم تحقيقه في تقليل الضوضاء والتميز بين المرشحات الكلاسيكية والمرشحات الأكثر تطوراً التي تطورت للتعامل مع التفاصيل الدقيقة. تأخذ هذه المرشحات في الاعتبار أوجه التشابه والمسافات بين العنصر الصوري المركزي وجيرانه، وتحافظ على حواف الصورة كميزات متقدمة، وبالاعتماد على قياسات الجودة (PSNR) و (SSIM)، تمت مقارنة نتائج المرشح وتبين أن المرشح المقترح يعطي أداء عالي في استعادة الصور تحت كثافات الضوضاء الغوسية المختلفة، حيث يعطي قيم (42.51) و (0.99) لـ (PSNR) و (SSIM) على التوالي مقارنة بالمرشح الثنائي الذيل ثانياً بـ (30.65) و (0.93) على التوالي.

معلومات البحث

تواريخ البحث:

تاريخ تقديم البحث: 16/2/2024
تاريخ قبول البحث: 12/4/2024
تاريخ رفع البحث على الموقع: 31/12/2024

الكلمات المفتاحية:

تقليل ضوضاء الصورة؛ استعادة الصورة؛
ضوضاء غاوس. مرشح المتوسط غير
المحلي؛ مرشح ثنائي.

للمراسلة:

محمد عبد الودود محمد

Mohamed.a.mohamed@coadec.uobaghdad.edu.iq

DOI: <https://doi.org/10.55562/jruc.s.v56i1.39>